Identification number: DOI: 10.1016/j.apsusc.2013.08.103
Official URL: http://dx.doi.org/10.1016/j.apsusc.2013.08.103

Surface integrity after pickling and anodization of Ti–6Al–4V titanium alloy

Eric Vermesse[a,b], Catherine Mabru[a], Laurent Arurault[b,*]

[a] Institut Clément Ader (ICA), Université de Toulouse, ISAE, Toulouse, France
[b] Université de Toulouse, Institut Carnot CIRIMAT, UMR CNRS-UPS-INP 5085, Université Paul Sabatier, 118, route de Narbonne, 31062 Toulouse cedex 9, France

A B S T R A C T

The surface integrity of Ti–6Al–4V titanium alloy was studied at different stages of surface treatments, especially pickling and compact anodization, through surface characteristics potentially worsening fatigue resistance.

No significant changes of the equiaxe microstructure were detected between sample core and surface, or after the pickling and anodization steps. Surface hydrogen and oxygen superficial contents were found to remain unchanged. Roughness characteristics (i.e. R_a, R_z but also local K_t factor) similarly showed only slight modifications, although SPM and SEM revealed certain random local surface defaults, i.e. pits about 400 nm in depth. Finally internal stresses, evaluated using X-ray diffraction, highlighted a significant decrease of the compressive internal stresses, potentially detrimental for fatigue resistance.

Keywords:
Titanium alloy
Pickling
Anodization
Roughness
Internal stresses

1. Introduction

Titanium alloys are increasingly used in the aeronautical industry due to their good mechanical properties and their low density. The most commonly used is Ti–6Al–4V because it is a good compromise between titanium's properties. However, additional surface treatment is usually required [1,2] to increase, for instance, superficial mechanical properties (i.e. tribological properties, wear resistance and superficial hardness), as well as to improve its behaviour with respect to corrosion by fluorided acidic solutions. Surface treatments on titanium alloys usually involve three main steps. The first is degreasing step which removes the oil and impurities on the surface, left by previous machining stages. The second is pickling commonly performed by chemically controlled corrosion typically in mixed hydrofluoric-nitric acid bath. The aim of this pre-treatment is to remove the natural passivating layer. Finally, the third stage is the main treatment, i.e. nowadays thermodiffusion treatments (nitriding, carburizing) or shot peening treatments [3–5]. Another simple and cost-effective treatment is anodization, creating either a compact top film or a porous one, including numerous mesopores [6,7]. Porous anodic films are currently being widely studied to prepare innovating photovoltaic cells [8,9] or to enhance osteointegration for bioapplications [10]. In contrast, compact anodic films are used both to colour the titanium surface [11–13] and to improve paint adhesion for aeronautic parts [2,14].

However, previous industrial and academic studies have unfortunately shown, especially for aluminium alloys (AA), that the anodization process causes significant modifications of the AA surface integrity and a subsequent decrease of the fatigue resistance [15–18]. To our knowledge, no research works have previously studied and explained the possible influence of surface treatments, especially pickling or the anodization, on fatigue resistance in titanium alloys. In the case of AA, decreased fatigue resistance after anodization is under investigation and has been mainly attributed to influent surface parameters such as: microstructure [19,20], uptake of embrittling chemical species [20–22], roughness [23,24] and internal stresses [25,26].

Microstructure has an important effect on the fatigue resistance of titanium alloys [19,20]. The main microstructural parameters are α grain size and the percentage and morphology of β phase. For example, a lamellar microstructure does not have the same mechanical properties as equiaxe microstructure [20]. Some surface treatments, such as nitriding or carburizing treatment, can also affect the microstructure and consequently the fatigue resistance.

Hydrogen, carbon, nitrogen and oxygen are the four main potential uptaking and embrittling species. Their respective effects are different but hydrogen embrittlement is well-known to affect mechanical properties of metal parts. This point is particularly critical as Ogawa et al. [27] clearly showed using hydrogen thermal desorption that the amount of absorbed hydrogen in a beta titanium alloy increased with immersion time in fluorided acid solutions.

* Corresponding author. Tel.: +33 561556148; fax: +33 561556163.
E-mail address: arurault@chimie.ups-tlse.fr (L. Arurault).

http://dx.doi.org/10.1016/j.apsusc.2013.08.103

The role of roughness on fatigue resistance of metal parts is well known and has been studied for a long time. Roughness can be significantly modified by surface treatments, such as for instance the pickling step. Thus, pickling of AA substrate often modifies the roughness through dissolution of microprecipitates initially included in the multiphase AA matrix [18]. On commercially pure titanium, pickling performed in a concentrated (48%) sulphuric acid bath is similarly used to increase roughness in order to promote osteo-integration [28].

Finally, internal stresses contribute to the average stress applied to the material and consequently its fatigue resistance. Internal stresses may be generated by mechanical treatment (shot peening, ball burnishing), thermal treatment (quenching, annealing) and/or (electro)chemical treatment (nitriding, anodization). For instance, anodization induces compressive or tensile internal stresses, whose intensities depend on the operational parameters of the electrochemical treatment [29–32].

In the present work, the aim was to study the influence of surface treatment (pickling and anodization) on surface integrity of Ti–6Al–4V titanium alloy, widely used for aircraft parts such as for example engine pylons.

Surface integrity was studied through surface characteristics potentially influencing fatigue resistance. Firstly the microstructure of Ti–6Al–4V alloy was carefully studied through two types of substrates, i.e. rolled sheet and forged bar. Secondly, this work only focussed on hydrogen and oxygen uptakes because carbon and nitrogen are not involved, either in pickling treatment or in anodization treatment. Then roughness was studied through R_a and R_z values but also an approach based on the local stress concentration factor (local K_t). Erratic and punctual defaults were observed and characterised to complete the morphological analysis. Finally, internal stresses were measured using XRD methods. These different characteristics were deeply studied at both steps of surface treatment (pickling, anodization) while endurance limit was finally evaluated in order to both clarify the surface changes and predict their potential impact on fatigue resistance.

2. Experimental

2.1. Surface preparation

The substrate material was Ti–6Al–4V titanium alloy. Its chemical composition in weight percent was: $5.5 < Al < 6.5\%$, $3.5 < V < 4.5\%$, $C \leq 0.08\%$, $O \leq 0.20\%$, $N \leq 0.05\%$, $Fe \leq 0.30\%$, $H \leq 0.0125\%$ with Ti accounting for the remainder. Two different substrates were used in this study to finally obtain three different surface states.

The first substrate was Ti–6Al–4V rolled sheet (45 mm × 60 mm × 1 mm). From this substrate, two surfaces were prepared: raw rolled sheet and polished sheet. The polished samples were obtained using 800, 1200, 2400 grade polishing paper discs and 6, 3 then 1 μm diamond paste polishing pads.

The second substrate was Ti–6Al–4V forged bar (length: 105 mm; diameter: 16 mm) turned (feed rate: 0.1 mm/revolution; cutting speed: 25 m/min) to obtain a fatigue specimen (working length: 20 mm; working diameter: 8 mm), that made up a third surface state.

All samples were degreased with ethanol and then acetone. They were then pickled in aqueous 20 w% HNO_3 and 2 w% HF mixed solution at 20 °C for 200 s without stirring.

Finally, the anodization was performed in an electrochemical cell, where the titanium substrate was used as anode and a lead plate as counter-electrode. The anodization was run for 2 min in the direct voltage mode (5–80 V) using a sulfuric acid solution (1 M) thermally regulated at 20 °C. Samples were rinsed with distilled water after each step.

2.2. Characterizations

The thickness of the anodic film was measured using a Bentham PVE300 reflectometer, with a TMc300 monochromator in the 300–900 nm wavelength range. For the anodic film, the refractive index provided by Diamanti et al. [11] was used.

Secondary Ion Mass Spectrometry (SIMS) surface and cross-sectional analysis were performed with a Cameca IMS 4F6 device. The area analysed was 150 μm × 150 μm using a 10 keV Cs^+ primary beam with 10–50 nA current range. It is important to note that this area of analysis was larger than the α and β grain sizes (maximum 40 μm^2).

Prior to microstructural observations, samples were dipped for 10 s in a mixed acid solution (4% HF; 3%HNO_3) at ambient temperature. Sample microstructures were observed with a scanning electron microscope (XL30 ESEM), while α and β grain sizes were estimated by analyzing SEM views with the free software ImageJ [33]. Additional observations of the sample microstructure were carried out using an optical microscope (OM) (Olympus GX 71).

Elementary chemical analyses were performed by energy-dispersive X-ray spectroscopy (Rondec-EDX) coupled with a SEM device, in order to obtain a semi-quantitative analysis of V, Ti, Al contents in both types of grains.

A Mahr perthometer PGK 120 (contact mode in ambient atmosphere, diamond tip with 2 μm radius) was used to access to the amplitude parameters of the roughness, i.e. here the roughness average (R_a) and roughness height (R_z), defined by:

$$R_a = \frac{1}{l}\int_0^l |z(x)|dx \tag{1}$$

with l the length of profile and $z(x)$ the profile height distribution with respect to mean line

$$R_z = \frac{1}{5}\left[\sum_{i=1}^{5}|(z_i)_{max}| + \sum_{j=1}^{5}|(z_j)_{min}|\right] \tag{2}$$

where $(z_i)_{max}$ and $(z_j)_{min}$ are respectively the five higher local maxima and lower local minima of the profile height distribution (z).

The R_a and R_z values shown in this paper were the average values, resulting from 4 to 40 measurements. Corresponding accuracy was low (about 0.01 μm) while the standard deviation was about 0.05 μm for R_a and 0.5 μm for R_z. Only R_a and R_z values were used in this paper but the final conclusion would remain the same with the other roughness indexes.

Unfortunately, roughness indexes do not always provide sufficient information to know the real effect of morphology on fatigue resistance [34,35]. Consequently, Suraratchaï et al. [34] and Shahzad et al. [16] proposed to use the local K_t to determine the morphology impact on the fatigue resistance. The specificity of the K_t parameter is that it takes depth and sharpness of the local defaults into account. Its calculation is based on roughness profile analysis and finite elements simulation [34]. In this method, roughness profile was filtered to extract its "useful" part, the cut length, assimilated to a_0 [23], being here close to 10 μm. Standard deviation for K_t is estimated to be equal to 0.03 for machined samples and 0.5 for laminate samples.

A scanning probe microscope (SPM-Bruker) in contact mode in ambient atmosphere with a 10 nm radius and a 10 μm long cantilever tip was used to characterise erratic local surface defaults at the micro- and nano-levels (50 μm × 50 μm).

The internal stresses were measured by X-ray diffraction (X-pert Philips device) using the well-known "$\sin^2\psi$ method" firstly introduced by Macherauch [36,37]. Measurements were only carried out on unpolished rolled samples because the XRD technique is unsuitable for cylindrical samples (like machined forged bar used

for fatigue specimen) and polishing can induce additional uncontrolled stresses. All measurements were performed in the laminate direction using a 213 diffraction ray with scanning angle (2θ) from 136° to 146°. The measurement of internal stresses was performed in a material depth depending on the XRD analysis operating parameters (angle, X-ray tube), but depth is usually considered as about the first 14 μm [38].

Preliminary fatigue tests were performed on a servo hydraulic machine MTS-810 at 10 Hz using a load ratio of 0.1. Specimen geometry, already used in previous works, was described for instance in Ref. [16]: gauge length was 20 mm and diameter was 8 mm. The specimens were machined from a unique bar. Three groups of seven specimens were tested: the first one without surface treatment, another one only pickled and the last one pickled and then anodized at 80 V.

3. Results and discussion

As mentioned in the introduction, surface integrity was studied through surface characteristics potentially influencing the fatigue resistance, i.e. microstructure, species uptake, roughness and internal stresses.

3.1. Microstructure

Ti–6Al–4V rolled sheet (First substrate) showed a fine isotropic equiaxe microstructure (Fig. 1), homogeneous through the whole thickness. The second substrate (Ti–6Al–4V forged bar) showed similar fine equiaxe-type microstructure in the radial direction (Fig. 2a) but also specifically long fine β grains oriented along the longitudinal direction (Fig. 2b). The average diameter of β grains was about 1 μm while the diameter of α grains was estimated to be about 5 μm.

Image analysis showed that the surface area of β grains is $10 \pm 2\%$ for both rolled samples and radial observation of the forged sample, and $7 \pm 2\%$ for the longitudinal direction of the forged sample. These results agree with the fact that (α + β) titanium alloys show β phase in the 5–20% range, especially close to 12% for the Ti–6Al–4V alloy [39].

There were no significant differences of microstructure between sample cores and their interfaces, i.e. in the last superficial one thousand microns. Moreover, no changes were experimentally observed after the pickling and anodization steps. These results were firstly explained by the similar chemical content and chemical distribution in both types of substrates. Secondly, both processes are indeed known to usually induce no changes of superficial microstructure because of the ambient or moderate operational temperatures used, contrary to thermodiffusion treatments (i.e. nitriding [5]) or high energy treatments (i.e. micro-arc oxidation, laser treatment [40,41]). So, using pickling and anodization, microstructure cannot be considered as a key parameter for potential fatigue resistance modification of Ti–6Al–4V titanium alloy.

3.2. Hydrogen and oxygen uptake

This work focussed on the uptake of hydrogen and oxygen both known to affect mechanical properties [42,43] and both involved in the pickling and the anodization processes, unlike carbon and nitrogen. To study the hydrogen storage capacity of the Ti–6Al–4V, temperature programmed desorption (TPD) and a volumetric sorption technique have been performed [44]. The diffusion kinetics of oxygen into Ti–6Al–4V substrate was measured by weight gain measurements, oxygen diffusion zone (ODZ) depth and hardness measurements on the cross-sections of oxidised alloy [45]. Using SIMS, Thair et al. [46] obtained the elemental (Ti, Al, V, N, O) depth profiles of passive layers of (un)implanted specimens of Ti–6Al–4 V, while Lamolle et al. [47] studied the impact of the pickling duration on the SIMS depth profiles of oxide, fluoride and hydride in the surface of commercially pure (cp) titanium.

In the present study, SIMS was selected as it is very sensitive and provides the elemental in-depth profiles of the passive layer and the beginning of the metal matrix. However, quantitative values were not obtained but the method was efficient to compare significant variations of the elements present.

Fig. 3 shows the oxygen profiles after each treatment, i.e. polishing, pickling (20 w% HNO_3–2 w% HF solution for 200 s) and anodization (at 80 V). For polished and pickled samples, the initial peaks at the extreme surface (sputerring time lower than 200 s) were attributed to passive layers. Sittig et al. [48] highlighted that the natural passive layer (before pickling) on Ti–6Al–4V alloy is usually made up of TiO_2, but also includes Al_2O_3 and V_2O_5. Lamolle et al. [47] pointed out that prolonging the pickling time (up to 150 s) in 0.2%HF caused a higher oxide content at the cp titanium passivation layer. For Ti–6Al–4V alloy, our results did not show such an increase, may be due to the different titanium substrate and the lack of oxidising compound (i.e. HNO_3) in the pickling solution used by Lamolle et al. [47].

For anodized samples, the profile first presents an increase and then reaches a plateau due to the formation of the anodic film, about 200 nm thick, according to:

$$Ti + 2H_2O \rightarrow TiO_2 + 4H^+ + 4e \quad (3)$$

Then there is a drastic decrease of the SIMS profile at about 1500 s of sputtering, clearly indicating the interface between the bottom of the anodic film and the top of the metal alloy.

After each treatment (polishing, pickling, anodizing), oxygen intensity in bulk material was very low, indicating that no oxygen uptake occurred in the bulk alloy. So, a potential decrease of fatigue resistance due to oxygen uptake [20], usually attributed to titanium hardening [49], is not expected in these conditions.

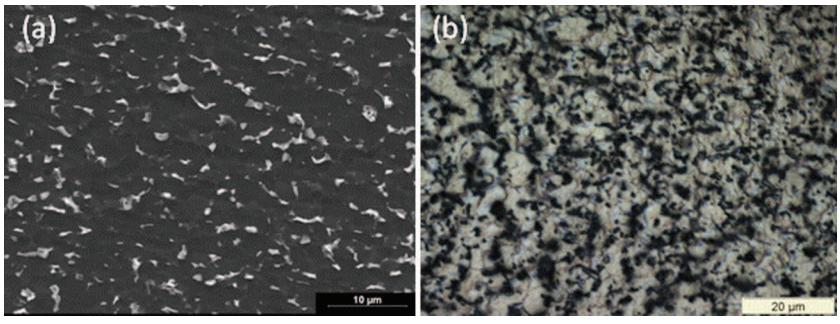

Fig. 1. (a) SEM view and (b) OM view of rolled sheet microstructure, previously pickled in a mixed 4 w%HF–3 w%HNO_3 solution for 10 s at ambient temperature.

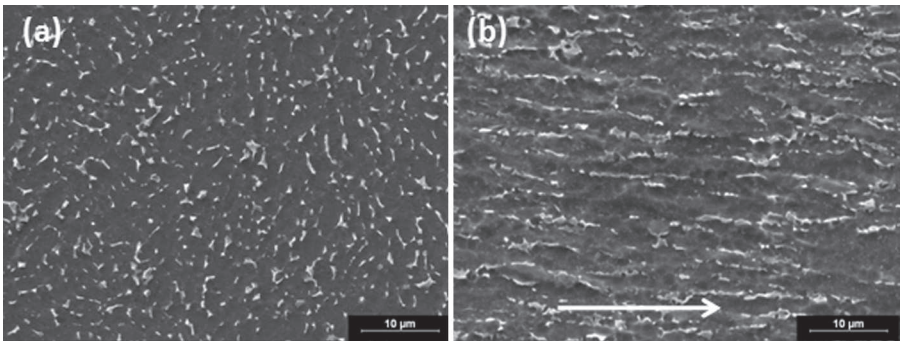

Fig. 2. SEM views (a) in radial direction and (b) in longitudinal direction (arrow) of forged bar microstructure, previously pickled in a mixed 4 w%HF–3 w%HNO_3 solution for 10 s at ambient temperature.

Fig. 3 also shows the hydrogen SIMS profile after each treatment, i.e. polishing, pickling and anodization. After polishing, the SIMS profile showed a high initial peak attributed to the hydration of the natural passive layer, mainly made up of TiO_2.

After pickling (20 w% HNO_3–2 w% HF solution for 200 s), the interfacial peak was clearly lower than the previous one (after polishing). This result could be explained by considering the possible pickling reactions occurring in 20 w% HNO_3 and 2 w% HF aqueous mixed solution:

$$6HF + TiO_2 \rightarrow 2H^+ + 2H_2O + TiF_6^{2-} \quad (4)$$

$$3HF + Ti \rightarrow 3/2H_2 + 3F^- + Ti^{3+} \quad (5)$$

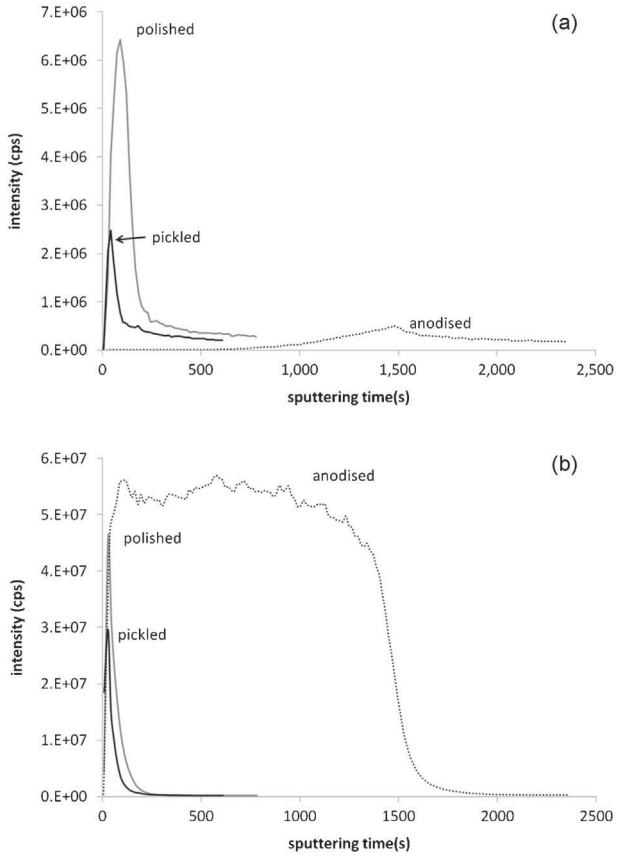

Fig. 3. (a) Hydrogen and (b) oxygen SIMS profiles obtained on rolled sample after three different steps: polishing then pickling (HNO_3–HF (20–2 w%) solution, 20 °C, 200 s) and finally anodization (80 V, 1 M H_2SO_4, 20 °C, 2 min).

Eq. (5) clearly shows that H_2 gas evolution can occur but also that titanium oxide reacts with fluoride anions. Thus, the decrease of the interfacial peak after pickling could perhaps be explained by the modification of the initial hydrated passive layer by the fluoride ions. Furthermore, Bijlmer [50] demonstrated that hydrogen uptake decreases with increasing nitric acid concentration. He showed in particular that, when the nitric acid content is higher than 20% in the pickling bath, hydrogen uptake became close to zero, due to a predominant re-passivation phenomenon. So, our results, obtained using 20 w%HNO_3–2 w%HF aqueous mixed pickling solution, are in good agreement with Bijlmer's work.

For an anodized sample (80 V, i.e. about 200 nm thick), the hydrogen profile increased from 750 s reaching a maximum at about 1500 s of sputtering. This maximum corresponded, as previously demonstrated for the oxygen depth profile, to the interface between the bottom of the anodic film and the top of the bulk metal alloy. Moreover, the area integration under the hydrogen profiles for pickled and anodized samples were the same, proving that anodization did not induce additional hydrogen uptake. Finally, hydrogen intensity in the bulk of the titanium alloy appeared low and identical after each treatment, confirming that no additional hydrogen inclusion was induced. In contrast, Lamolle et al. [47] showed a significant penetration depth of hydride (deeper than one micron) but used 0.2%HF alone (without nitric acid) aqueous solution as pickling bath, i.e. without re-passivation phenomenon.

Additional SIMS surface mapping (Fig. 4) was then performed to clarify the hydrogen state, which is a key factor in hydrogen embrittlement [51] Diffusive hydrogen indeed has a different effect than

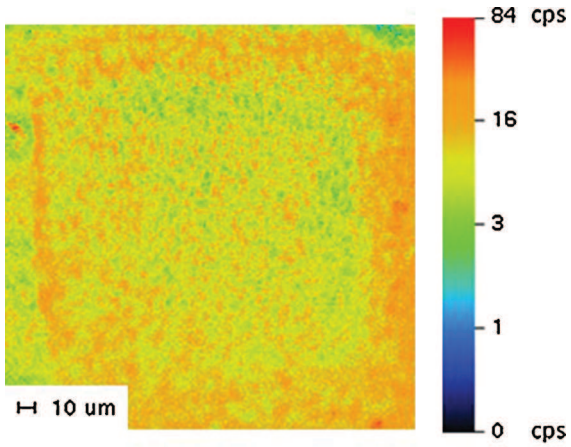

Fig. 4. SIMS surface mapping of hydrogen on a polished and then pickled sample (HNO_3–HF (20–2 w%) solution, 20 °C, 200 s). In the middle of the sample appears a sputtered crater a few microns in depth.

Table 1
Roughness and local K_t values for rolled and polished, rolled and machined samples before and after pickling (HNO_3–HF (20–2 w%) solution, 20 °C, 200 s).

	Polished			Rolled			Machined		
	Initial (μm)	Etched (μm)	Variation (%)	Initial (μm)	Etched (μm)	Variation (%)	Initial (μm)	Etched (μm)	Variation (%)
R_a	0.06	0.08	33	0.42	0.42	0	1.01	0.96	−5.3
R_z	0.28	0.58	107	2.72	2.70	−1.8	4.91	4.62	−6.4
K_t	1	1	0	2.31	2.16	−6.5	1.15	1.16	0.9

hydride precipitates [52,53], that decrease the ductility of the material [54]. The sample was in fact divided into two zones in order to compare the top surface and the "bulk" material (Fig. 4): in the middle was located a sputtered crater a few microns in depth and around the top surface of the anodic film. The colour homogeneity attested that hydrogen was uniformly distributed through the film, i.e. both on the surface and in the bulk of the anodic film. Considering that no chemical heterogeneity was detected, it is assumed that in the present case there were no hydride precipitates but only diffusive hydrogen. Nakasa and Satoh [21] claimed that diffusive hydrogen is usually incorporated into the β-phase but is less detrimental than the hydride from the α-phase, that can become a crack nucleation and propagation path under loading.

Thus, the oxygen and hydrogen uptakes were very limited in Ti–6Al–4V alloy using such surface treatments (polishing, pickling, anodization) in our operating conditions. So, the effect of variations in the hydrogen and oxygen contents will be considered as negligible from the fatigue resistance point of view.

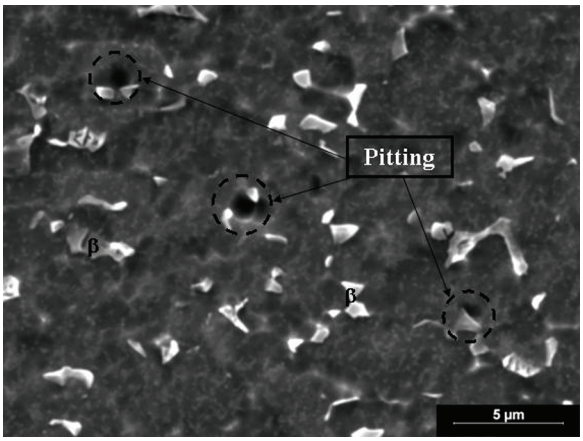

Fig. 5. SEM surface view of rolled sample, polished and then pickled (HNO_3–HF (20–2 w%) solution, 20 °C, 200 s) showing pits and β-phase (white parts).

3.3. Average roughness values and local default measurements

The morphological modifications of the surface which can impact the fatigue resistance were then analysed. Average roughness values (R_a and R_z) were firstly analysed to have a global description of the surface modifications. Considering that the real impact of surface morphology on fatigue resistance is incompletely described through roughness indexes [34,35], local K_t values were secondly obtained. However, these values do not directly take local and random defaults into account. That is why SEM and SPM analysis were performed (on polished surfaces) to determine the occurrence of any possible localised defaults.

3.3.1. On pickled samples

Roughness values (R_a and R_z) were measured before and after pickling on three types of samples (rolled, rolled then polished, machined) with different initial roughness (Table 1).

For rolled then polished samples, R_a and R_z changed from 0.06 ± 0.01 μm and 0.28 ± 0.01 μm respectively before pickling to 0.08 ± 0.01 μm and 0.58 ± 0.02 μm after pickling. So, R_a increased about 33% and R_z about 107% (Table 1). These are high relative increases but the final roughness values stayed very low. When the initial roughness was higher, i.e. for rolled or machined samples, roughness indexes (measured perpendicularly to the roll direction and in the longitudinal direction respectively) did not increase or even showed a slight decrease (Table 1). For example, changes were close to 0% for rolled sample with initial R_a of 0.42 ± 0.07 μm, while R_a and R_z decreased, about −5.3% and −6.4% respectively, after pickling the machined sample. However, these roughness index changes were lower than standard deviation, i.e. SD > 15%.

Roughness changes (increase or decrease) can result from different phenomena: preferential morphological dissolution of specific zones (tip/hollow), preferential chemical dissolution of specific phases of the alloy matrix, formation of local corrosion pits, etc.

Firstly, preferential morphological dissolution of the peaks that were more exposed to the pickling bath can occur. Indeed, the dissolution rate would be probably higher on peaks compared with the rate observed in hollows since mass transport and bath renewal would be more difficult in hollows.

Secondly, there is preferential chemical dissolution of α phase, as shown by SEM (Fig. 5) where β grains are higher than the α phase. SPM analysis (Fig. 6) provided an approximate height of about 800 nm for the β phase, i.e. lower than the average diameter of the β-grain (≈1 μm). This preferential chemical dissolution could be explained by considering the respective chemical compositions of both α and β phases. Indeed the β-phase has a higher concentration in vanadium and the α-phase a higher aluminium content (Table 2). Knowing that the standard potential of aluminium and vanadium are respectively −1.66 V/SHE and −1.13 V/SHE, the β-phase can be considered as more noble (containing more vanadium) than the α-phase with less vanadium and more aluminium.

Thirdly, another way to increase roughness is pitting. However, Fig. 6 shows that pits were local and less than 1 μm in diameter, and the pit density was evaluated at about one pit for 200 μm^2. Pits can be found at the grain boundaries, i.e. the interface between α and β phases, or also in the middle of α grains. SPM analysis revealed pit depth of about 400 nm (Fig. 6). So, preferential chemical dissolution and pitting phenomena resulting from the pickling step induced faults (respectively about 800 and 400 nm) lower than the roll roughness (R_z = 2.70 μm in Table 1). Both these types of defaults could explain the roughness changes (R_z = 0.58 μm in Table 1) in polished substrate.

Surprisingly, local K_t remained unchanged in polished and machined samples, while rolled samples showed a K_t decrease (−6.5%). Even though its variation seems to be significant, it is clearly lower than standard deviation on local K_t analysis, which reached 30% for the rolled sample. The low influence of faults on

Table 2
EDX evaluation of aluminium and vanadium contents in the α and β phases in rolled Ti–6Al–4V titanium alloy.

	% Al	%V
α Phase	5.6	2.9
β Phase	4.8	12.4

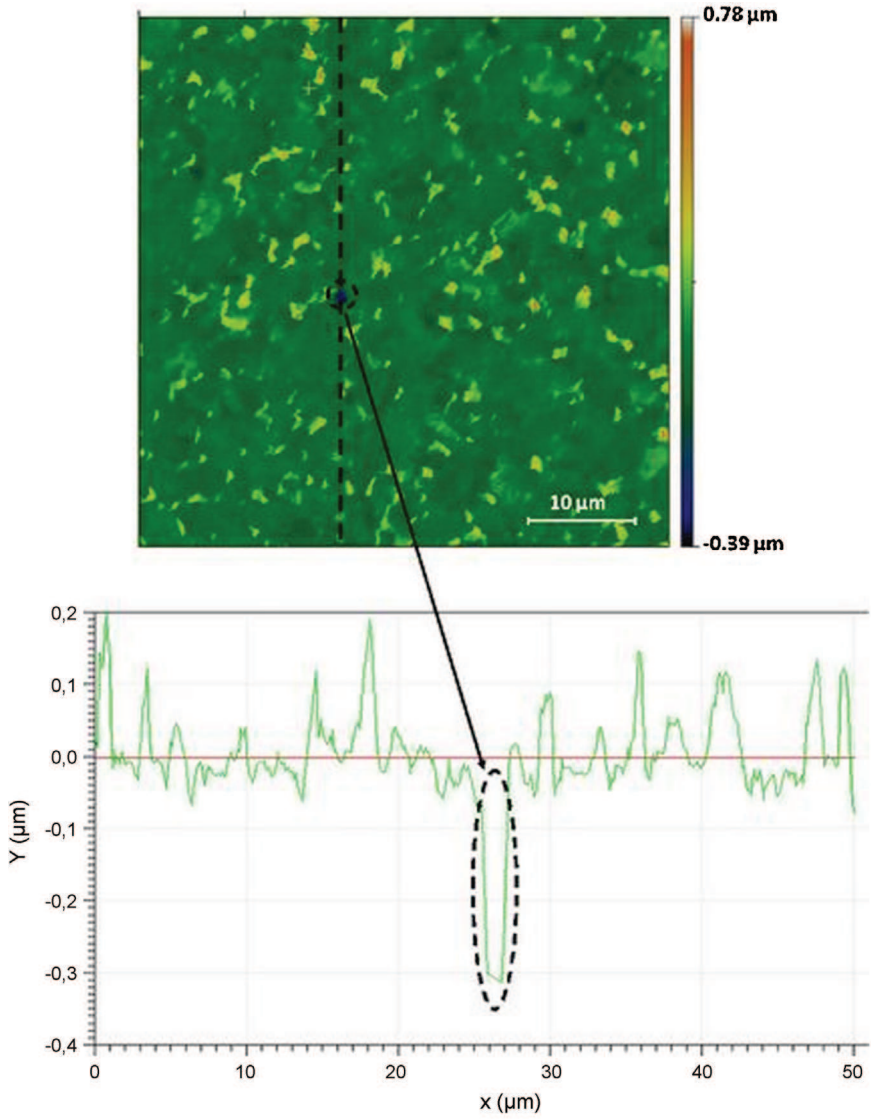

Fig. 6. SPM surface mapping and profile of polished then pickled sample (HNO_3–HF (20–2 w%) solution, 20 °C, 200 s) showing a pit.

local K_t value can be explained by too shallow sharpness and depth of faults. For instance, in rolled sample, defaults had a lower density and/or a lower depth than the initial guide marks from the rolling process (Table 1).

3.3.2. On anodized samples

R_a, R_z, K_t changes after anodization of rolled samples, performed at different constant voltages (5–80 V) are reported in Fig. 7, i.e. as function of the thickness of the compact anodic film in the 16–195 nm range (Table 3). R_a values changed significantly, maximal variations being about 7% between the thinnest and the thickest films. Although significant, the variations stayed very low. In the case of R_z values, the changes were larger (up to 8%) but they depended more on local faults. Local K_t changes were higher than R_z, but the corresponding standard deviation was large (30%) due to irregular roughness profiles.

So, no effect of the anodization voltage (i.e. the compact film thickness in the 16–195 nm range) was noted on the roughness or local K_t.

Complementary SEM surface views showed that the morphology of the anodized surface was unchanged whatever the anodic film thickness. For instance, SEM observations (Fig. 8) of the top surface of the thickest anodic oxide film clearly showed pits similar to the previous ones resulting from pickling step (Fig. 5); besides the pit density remained the same. However, additional concretions appeared (Fig. 8) on the surface of this anodic film but only when prepared at the highest voltage (80 V). The concretions occurring at the high voltage required to obtain thick layers, probably resulted from the occurrence of micro-sparks during the anodization.

Table 3
Thickness variation as a function of direct anodization voltage (1 M H_2SO_4, 20 °C, 2 min.) on rolled then pickled samples (HNO_3–HF (20–2 w%) solution, 20 °C, 200 s). Thicknesses were obtained using reflectometry analysis.

U (V)	e (nm)
5	16
20	60
35	94
50	130
65	164
80	195

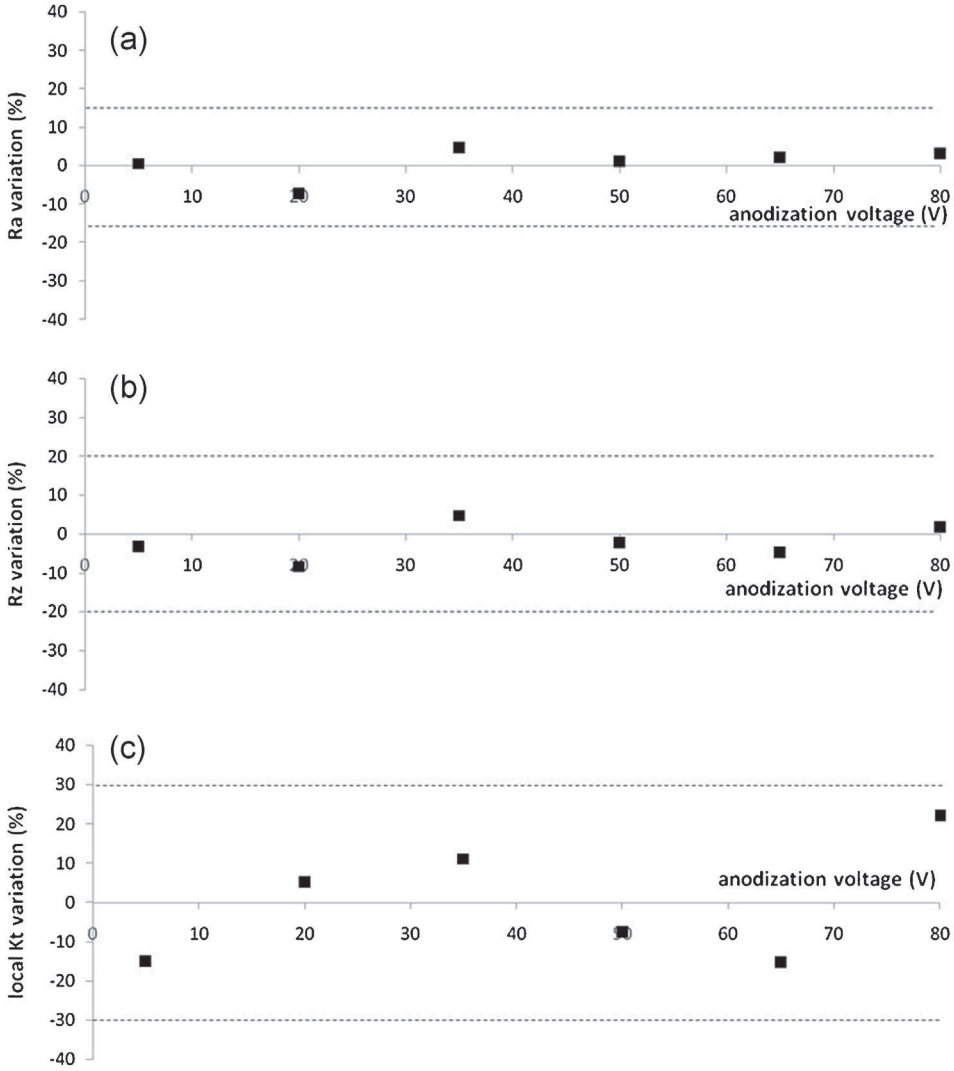

Fig. 7. Changes of (a) R_a (b) R_z average roughness values and (c) local K_t values as a function of the anodization voltage (5–80 V), i.e. the thickness of the film (16–195 nm) prepared on rolled sample pickled (HNO_3–HF (20–2 w%) solution, 20 °C, 200 s) then anodized (1 M H_2SO_4, 20 °C, 2 min). The dotted lines correspond to standard deviation.

To sum up, the growth of the anodic film on Ti–6Al–4V alloy induced no or slight modifications of the roughness (R_a, R_z) and local default (K_t) parameters. They appeared almost unchanged, compared with those obtained before anodization, i.e. after pickling. So, the growth of the compact film could be considered as simply arising from the previous roughness and local default characteristics, and could have no additional influence on fatigue resistance from this point of view.

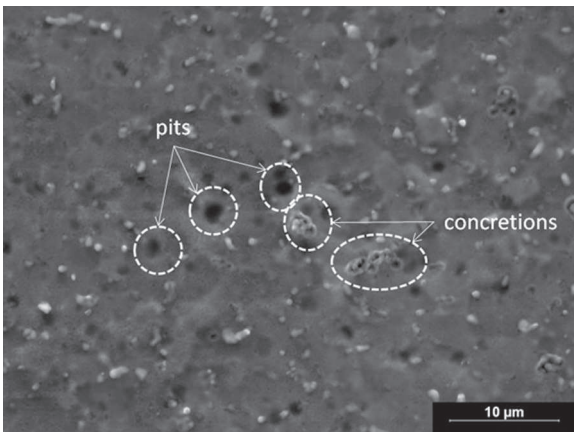

Fig. 8. SEM surface view of rolled sample, polished and pickled (HNO_3–HF (20–2 w%) solution, 20 °C, 200 s) then anodized (80 V, 1 M H_2SO_4, 20 °C, 2 min).

3.4. Internal stresses

There are many techniques to measure internal stress. Among them, the most widespread are X-ray diffraction (XRD) analysis [55,56], incremental hole drilling analysis [57] or beam bending analysis [58,59]. The XRD analysis was selected in our study for three main reasons: it is the only non-destructive technique allowing analysis of the internal stress and then subsequent fatigue testing on the same sample; the second reason is that, unlike beam bending analysis, the measurement can be carried out on thick samples and thirdly the data for stress calculation are easily available.

Rolled sheets showed initial compressive internal stresses (-198 ± 50 MPa) in the laminate direction (Fig. 9) in agreement with Abdelkhalek et al. [60]. Then the pickling step halved the internal stresses (-100 ± 50 MPa). Knowing that in this case the pickling removed about 3 μm thickness from the outer surface suggests that the internal stresses were mainly located at the outer surface and that a stress gradient could be located in the first microns

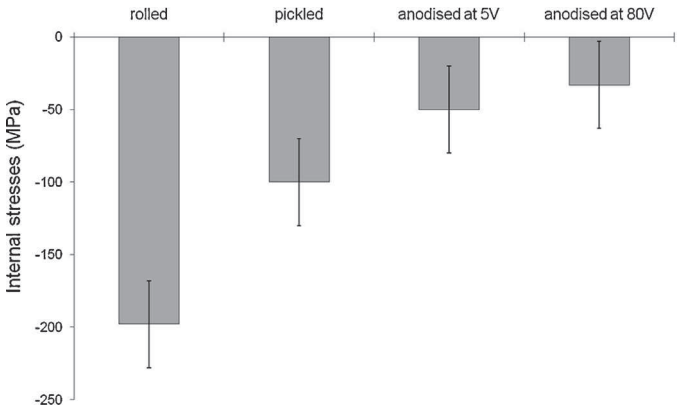

Fig. 9. Evolution of internal stresses obtained on four rolled samples after different surface treatments: rolled, rolled then pickled (HNO_3–HF (20–2 w%) solution, 20 °C, 200 s), rolled then pickled and finally anodized at 5 V (1 M H_2SO_4, 20 °C, 2 min) and a rolled then pickled and finally anodized at 80 V (1 M H_2SO_4, 20 °C, 2 min).

of depth. Moreover, stress is seen to result from anodization, for the thinnest (16 nm at 5 V) and thickest (195 nm at 80 V) films, i.e. -50 ± 40 MPa and -39 ± 35 MPa respectively Fig. 9; the values can be considered as similar, and were clearly lower than the previous ones obtained after pickling (-100 ± 50 MPa). Moreover, the anodic film was mainly amorphous and consequently did not contribute to the XRD analysis. So, the measured remaining compressive stresses were probably located at the metal/oxide interface, in agreement with the mechanism proposed by Nelson and Oriani [31]. They explain that the anodization induces additional tensile stress (up to 50 MPa) due to vacancies generated by the formation and the migration of titanium ions at the metal/oxide interface. Such compressive stresses, detected at each step of the surface treatments (especially pickling and anodization) could clearly have a detrimental effect on the fatigue resistance [25,61,62].

3.5. Endurance limit

Fatigue life is divided in three parts: crack nucleation, crack propagation and ductile failure. Crack nucleation occurs principally at the surface. Thus, it is highly sensitive to surface integrity.

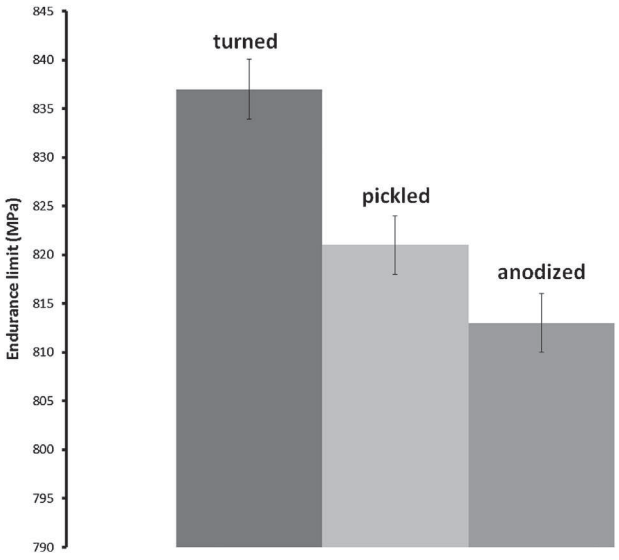

Fig. 10. Endurance limit of three samples: turned, turned then pickled (HNO_3–HF (20–2 w%) solution, 20 °C, 200 s), turned, pickled and finally anodized at 80 V (1 M H_2SO_4, 20 °C, 2 min).

Furthermore, it represents the main part of fatigue life when the number of cycles is high. That is why, endurance limits which corresponding to fatigue failure at 10^7 cycles are closely linked with surface integrity. The experimental values of endurance limit as a function of surface treatments are reported on Fig. 10. A decrease of endurance limit was observed after pickling and anodizing. The decrease was about 20 MPa after pickling and 10 MPa after anodizing. These variations were meaningful but appeared quite low in comparison with internal stresses modifications measured in rolled specimens. It must be noted that these results are preliminary results and that further work is needed to precisely investigate fatigue behaviour and fatigue models including the effect of residual stresses.

Nevertheless, this preliminary fatigue study is in good agreement with the previous results on surface integrity and confirms that in this case changes of internal stresses modify the endurance limit. These results should be taken into account to improve the surface treatments from a fatigue point of view.

4. Conclusion

The surface integrity of Ti–6Al–4V alloy was studied through surface characteristics (microstructure, hydrogen and oxygen uptakes, roughness and local surface defaults, internal stresses) potentially influencing fatigue resistance. These surface characteristics were studied in detail after both surface treatments (pickling, anodization). The main conclusions were the following:

Both rolled and forged Ti–6Al–4V substrates showed equiaxe microstructures, including about $10 \pm 2\%$ β grains. No significant microstructural changes were detected between sample core and surface, or after the pickling and anodization steps.

SIMS analysis revealed then that no oxygen and hydrogen uptake occurred in the bulk alloy, irrespective of the surface treatment (pickling, anodizing). It was also assumed that no hydride precipitates were formed but only diffusive hydrogen was present in our experimental conditions.

The morphological modifications of the surface were then analysed through average roughness (R_a, R_z) or local K_t parameters, as well as using SEM and SPM techniques to detect some possible localised and random faults. After pickling, local K_t was not affected while there were slight roughness changes, attributed to different phenomena: preferential morphological dissolution of peaks, preferential chemical dissolution of the less noble α-phase and formation of local pits. No effect of the anodization compact film thickness in the 16–195 nm range was found on either the roughness parameters or local K_t.

In contrast, XRD analysis clearly showed that there were compressive internal stresses and that their values significantly decreased (from -198 ± 50 MPa to -39 ± 30 MPa) after each step of the surface treatment. The internal stresses were mainly located at the metal/oxide interface.

Moreover, preliminary fatigue tests revealed a significant decrease of endurance limit after each surface treatment. Finally, this surface integrity analysis showed that the modification of the initial compressive internal stresses could be a key-parameter, potentially explaining the decrease of the endurance limit after each surface treatment (pickling and anodization) on the Ti–6Al–4V titanium alloy.

Acknowledgments

The authors thank Claude Armand for his help in performing the SIMS analysis and Pascal Lamesle for the internal stress measurements, as well as Peter Winterton for his helpful comments.

References

[1] A. Zhecheva, W. Sha, S. Malinov, A. Long, Enhancing the microstructure and properties of titanium alloys through nitriding and other surface engineering methods, Surf. Coat. Technol. 200 (2005) 2192–2207.
[2] G.W. Critchlow, D.M. Brewis, Review of surface pretreatments for titanium alloys, Int. J. Adhes. Adhes. 15 (1995) 161–172.
[3] D.G. Bansal, O.L. Eryilmaz, P.J. Blau, Surface engineering to improve the durability and lubricity of Ti–6Al–4V alloy, Wear 271 (2011) 2006–2015.
[4] O.I. Yaskiv, I.M. Pohrelyuk, V.M. Fedirko, D. Bok Lee, O.V. Tkachuk, Formation of oxynitrides on titanium alloys by gas diffusion treatment, Thin Solid Films 519 (2011) 6508–6514.
[5] I.M. Pohrelyuk, V.M. Fedirko, O.V. Tkachuk, R.V. Proskurnyak, Corrosion resistance of Ti–6Al–4V alloy with nitride coatings in Ringer's solution, Corros. Sci. 66 (2013) 392–398.
[6] J.M. Macak, H. Tsuchiya, L. Taveira, A. Ghicov, P. Schmuki, Self-organized nanotubular oxide layer on Ti–6Al–7Nb and Ti–6Al–4V formed by anodization in NH_4F solution, J. Biomed. Mat. Res. 75 (2005) 928–933.
[7] V. Zwilling, M. Aucouturier, E. Darque-Ceretti, Anodic oxidation of titanium and TA6V alloy in chromic media: an electrochemical approach, Electrochem. Acta 45 (1999) 921–929.
[8] K.Y. Lee, J.Y. Kim, H.Y. Kim, Y.J. Lee, Y.S. Tak, D. Kim, P. Schmuki, Effect of electrolyte conductivity on the formation of nanotubular TiO_2 photoanode for a dye-sensitized solar cell, J. Korean Phys. Soc. 54 (2009) 1027–1031.
[9] L. Cao, C. Wu, Q. Hu, T. Jin, B. Chi, J. Pu, L. Jian, Double-layer structure photoanode with TiO_2 nanotubes and nanoparticles for dye-sensitized solar cells, J. Am. Ceram. Soc. 96 (2013) 549–554.
[10] R. Chiesa, E. Sandrini, M. Santin, G. Rondelli, A. Cigada, Osteointegration of titanium and its alloys by anodic spark deposition and other electrochemical techniques: a review, J. Appl. Biomater. Biomech. 1 (2003) 91–107.
[11] M.V. Diamanti, B. Del Curto, M.P. Pedeferri, Interference colors of thin oxide layers on titanium, Color Res. Appl. 33 (3) (2008) 221–228.
[12] S. Van Gils, P. Mast, E. Stijns, H. Terryn, Colour properties of barrier anodic oxide films on aluminium and titanium studied with total reflectance and spectroscopic ellipsometry, Surf. Coat. Technol. 185 (2004) 303–310.
[13] Y.T. Sul, C.B. Johansson, Y. Jeong, T. Albrektsson, The electrochemical oxide growth behaviour on titanium in acid and alkaline electrolytes, Med. Eng. Phys. 23 (2001) 329–346.
[14] F. Dalard, C. Montella, J. Gandon, Adherence of paints on titanium: study and characterization of oxide films, Surf. Technol. 8 (1979) 203–224.
[15] B. Lonyuk, I. Apachitei, J. Duszczyk, The effect of oxide coatings on fatigue properties of 7475-T6 aluminum alloy, Surf. Coat. Technol. 201 (2007) 8688–8694.
[16] M. Shahzad, M. Chaussumier, R. Chieragatti, C. Mabru, F. Rezai-Aria, Influence of surface treatments on fatigue life of Al 7010 alloy, J. Mater. Process. Technol. 210 (2010) 1821–1826.
[17] M. Shahzad, M. Chaussumier, R. Chieragatti, C. Mabru, F. Rezai-Aria, Surface characterization and influence of anodizing process on fatigue life of Al 7050 alloy, Mater. Des. 32 (2011) 3328–3335.
[18] M. Shahzad, M. Chaussumier, R. Chieragatti, C. Mabru, F. Rezai-Aria, Effect of sealed anodic film on fatigue performance of 2214-T6 aluminium alloy, Surf. Coat. Technol. 206 (2012) 2733–2739.
[19] R. Boyer, G. Welsch, E.W. Collins (Eds.), Materials Properties Handbook: Titanium Alloys, fourth edition, ASM International, Materials Park, OH, 2007.
[20] G. Lütjering, J.C. Williams, Titanium, Springer, Berlin, 2003.
[21] K. Nakasa, H. Satoh, The effect of hydrogen-charging on the fatigue crack propagation behavior of β-titanium alloys, Corros. Sci. 38 (1996) 457–468.
[22] W.J. Evans, M.R. Bathe, Hydrogen and fatigue behaviour in a near alpha titanium alloy, Scr. Metall. Mater. 32 (1995) 1019–1024.
[23] M.H. El Haddad, T.H. Topper, K.N. Smith, Prediction of non propagating cracks, Eng. Frac. Mech. 11 (1979) 573–584.
[24] M. Chaussumier, C. Mabru, M. Shahzad, R. Chieragatti, F. Rezai-Aria, A predictive fatigue life model for anodized 7050 aluminium alloy, Int. J. Fatigue 48 (2013) 205–213.
[25] L. Wagner, G. Luetjering, Influence of shot peening on the fatigue behavior of titanium alloys, in: 1st International Conference on Shot Peening, Paris, 1981, pp. 453–460.
[26] M.N. James, D.J. Hughes, Z. Chen, H. Lombard, D.G. Hattingh, D. Asquith, J.R. Yates, P.J. Webster, Residual stresses and fatigue performance, Eng. Fail. Anal. 14 (2007) 384–395.
[27] T. Ogawa, K. Yokoyama, K. Asaoka, J. Sakai, Hydrogen absorption behavior of beta titanium alloy in acid fluoride solutions, Biomaterials 25 (2004) 2419–2425.
[28] S. Ban, Y. Iwaya, H. Kono, H. Sato, Surface modification of titanium by pickling in concentrated sulfuric acid, Dent. Mater. 22 (2006) 1115–1120.
[29] N.B. Pilling, R.E. Bedworth, The oxidation of metals at high temperatures, J. Inst. Metals 29 (1923) 529.
[30] L.C. Archibald, Internal stresses formed during the anodic oxidation of titanium, Electrochim. Acta 22 (1977) 657.
[31] J.C. Nelson, R.A. Oriani, Stress generation during anodic oxidation of titanium and aluminum, Corros. Sci. 34 (1993) 307–326.
[32] J.-D. Kim, S.-I. Puyn, M. Seo, Effect of hydrogen on stresses in anodic oxide film on titanium, Electrochim. Acta 48 (2003) 1123–1130.
[33] C.A. Schneider, W.S. Rasband, K.W. Eliceiri, NIH Image to ImageJ: 25 years of image analysis, Nat. Methods 9 (2012) 671–675.
[34] M. Suraratchaï, J. Limido, C. Mabru, R. Chieragatti, Modelling the influence of machined surface roughness on the fatigue life of aluminium alloy, Int. J. Fatigue 30 (2008) 2119–2126.
[35] S.K. Às, B. Skallerud, B.W. Tveiten, Surface roughness characterization for fatigue life predictions using finite element analysis, Int. J. Fatigue 30 (2008) 2200–2209.
[36] H.K. Tonshoff, B. Karpuschewski, A. Mohlfeld, H. Seegers, Influence of stress distribution on adhesion strength of sputtered hard coatings, Thin Solid Films 332 (1998) 146–150.
[37] I.S. Jawahir, E. Brinksmeier, R. M'Saoubi, D.K. Aspinwall, J.C. Outeiro, D. Meyer, D. Umbrello, A.D. Jayal, Surface integrity in material removal processes: recent advances, CIRP Ann. – Manuf. Technol. 60 (2011) 603–626.
[38] D. Puerta Velasquez, A. Tidu, B. Bolle, P. Chevrier, J.J. Fundenberger, Sub-surface and surface analysis of high speed machined Ti–6Al–4V alloy, Mater. Sci. Eng. A 527 (2010) 2572–2578.
[39] J.W. Elmer, T.A. Palmer, S.S. Babu, E.D. Specht, In situ observations of lattice expansion and transformation rates of α and β phases in Ti–6Al–4V, Mater. Sci. Eng. A 391 (2005) 104–113.
[40] A.L. Yerokhin, X. Nie, A. Leyland, A. Matthews, Characterisation of oxide films produced by plasma electrolytic oxidation of a Ti–6Al–4V alloy, Surf. Coat. Technol. 130 (2000) 195–206.
[41] L.E. Murr, S.A. Quinones, S.M. Gaytan, M.I. Lopez, A. Rodela, E.Y. Martinez, D.H. Hernandez, E. Martinez, F. Medina, R.B. Wicker, Microstructure and mechanical behavior of Ti–6Al–4V produced by rapid-layer manufacturing, for biomedical applications, J. Mechan. Behav. Biomed. Mater. 2 (2009) 20–32.
[42] R.W. Judy, I.L. Caplan, F.D. Bogar, Effects of oxygen and iron on the environmental and mechanical properties of unalloyed titanium, in: Proceeding of 7th World Titanium Conference, San Diego, 1992, pp. 2073–2081.
[43] M.R. Bache, W.J. Evans, M. McElhone, The effects of environment and internal oxygen on fatigue crack propagation in Ti–6Al–4V, Mater. Sci. Eng. A234–236 (1997) 918–922.
[44] J.L. Blackburn, P.A. Parilla, T. Gennett, K.E. Hurst, A.C. Dillon, M.J. Heben, Measurement of the reversible hydrogen storage capacity of milligram Ti–6Al–4V alloy samples with temperature programmed desorption and volumetric techniques, J. Alloys Compd. 454 (2008) 483–490.
[45] H. Guleryuz, H. Cimenoglu, Oxidation of Ti–6Al–4V alloy, J. Alloys Compd. 472 (2009) 241–246.
[46] L. Thair, U.K. Mudali, S. Rajagopalan, R. Asokamanic, B. Raj, Surface characterization of passive film formed on nitrogen ion implanted Ti–6Al–4V and Ti–6Al–7Nb alloys using SIMS, Corros. Sci. 45 (2003) 1951–1967.
[47] S.F. Lamolle, M. Marta, M. Rubert, H.J. Haugen, S.P. Lyngstadaas, J.E. Ellingsen, The effect of hydrofluoric acid treatment of titanium surface on nanostructural and chemical changes and the growth of MC3T3-E1 cells, Biomaterials 30 (2009) 736–742.
[48] C. Sittig, M. Textor, D. Spencer, M. Wieland, P.H. Valloton, Surface characterization of implant materials c.p. Ti, Ti–6Al–7Nb and Ti–6Al–4V with different pretreatment, J. Mater. Scie. Mater. Med. 10 (1999) 35–46.
[49] W. Liu, G. Welsch, Effects of oxygen and heat treatment on the mechanical properties of alpha and beta titanium alloys, Metall. Trans. A 19A (1988) 1121–1125.
[50] P.F.A. Bijlmer, Pickling titanium in hydrofluoric-nitric acid, Met. Finishing 68 (1970) 64–72.
[51] K. Yokoyama, T. Ogama, K. Asaoka, J. Sakai, Hydrogen absorption of titanium and nickel-titanium alloys during long-term immersion in neutral fluoride solution, J. Biomed. Mater. Res. 78B (2006) 204–210.
[52] A. Nagaoka, K. Yokoyama, J. Sakai, Evaluation of hydrogen absorption behaviour during acid pickling for surface modification of commercial pure Ti, Ti–6Al–4V and Ni–Ti superelastic alloys, Corros. Sci. 52 (2010) 1130–1138.
[53] C.L. Briant, Z.F. Wang, N. Chollocoop, Hydrogen embrittlement of commercial purity titanium, Corros. Sci. 44 (2002) 1875–1888.
[54] D. Hardie, S. Ouyang, Effect of hydrogen and strain rate upon the ductility of mill-annealed Ti-6Al-4V, Corros. Sci. 41 (1999) 155–177.
[55] B.R. Sridhar, D. Mehta, K.A. Padmanabhan, Effect of recrystallisation on the residual stress pattern and fatigue behaviour of titanium alloy IMI-685, J. Mater. Process. Technol. 138 (2003) 284–290.
[56] H. Lee, S. Mall, S. Sathish, M.P. Blodgett, Evolution of residual stresses in a stress-free titanium alloy subjected to fretting fatigue, Mater. Lett. 60 (2006) 2222–2226.
[57] C. Cellard, D. Retrainta, M. François, E. Rouhaud, D. Le Saunier, Laser shock peening of Ti-17 titanium alloy: influence of process parameters, Mater. Sci. Eng. A 532 (2012) 362–372.
[58] Y. Goueffon, C. Mabru, M. Labarrère, L. Arurault, C. Tonon, P. Guigue, Mechanical behavior of black anodic films on 7175 aluminium alloy for space applications, Surf. Coat. Technol. 204 (2009) 1013–1017.
[59] X.L. Peng, Y.C. Tsui, T.W. Clyne, Stiffness, residual stresses and interfacial fracture energy of diamond films on titanium, Diamond Relat. Mater. 6 (1997) 1612–1621.
[60] S. Abdelkhalek, P. Montmitonnet, N. Legrand, P. Buessler, Coupled approach for flatness prediction in cold rolling of thin strip, Int. J. Mechan. Sci. 53 (2011) 661–675.
[61] D.W. Schwach, Y.B. Guo, A fundamental study on the impact of surface integrity by hard turning on rolling contact fatigue, Int. J. Fatigue 28 (2006) 1838–1844.
[62] G.A. Webster, A.N. Ezeilo, Residual stress distributions and their influence on fatigue lifetimes, Int. J. Fatigue 23 (2001) S375–S383.